CHAPTER VII
NAPHTHALENE STEAM REFORMING OVER Mn-DOPED CeO_2-ZrO_2 SUPPORTED NICKEL CATALYSTS*

7.1 Abstract

In this study, the catalytic activity of nickel supported on $Ce_{0.75}Zr_{0.25-x}Mn_xO_2$ (x = 0, 0.10, 0.20 and 0.25) mixed oxide catalysts prepared by urea hydrolysis and incipient wetness impregnation was investigated for steam reforming of naphthalene selected as a model compound for biomass-derived tar. The results showed that nickel supported on $Ce_{0.75}Zr_{0.25-x}Mn_xO_2$ mixed oxide catalysts exhibit good activity for naphthalene steam reforming. It was found that the amount of carbon deposition reduced substantially when Mn was introduced to the CeO_2-ZrO_2 mixed oxide. This might be due to the fact that the incorporation of manganese ions into the ceria lattice would improve the oxygen storage capacity and the oxygen mobility on the surface of mixed oxides, resulting in enhancing the gasification of the deposited carbon.

7.2 Introduction

Biomass gasification is a promising technology for producing CO- and H_2-rich gases to be used for methanol or Fischer-Tropsch synthesis, chemical production or electricity generation (turbines, gas engines, or fuel cells). However, the presence of heavy organic impurities in the flue gas, i.e. tar, is the main technical barrier in the development of biomass gasification processes (Sutton *et al.*, 2001; Zhang *et al.*, 2004). Since tar is a complex mixture of heavy aromatics, it often causes various difficulties to the processing equipment, for instance, condensation or formation of aerosols. Moreover, tar is considered dangerous as a carcinogenic and possibly mutagenic substance (Abu El-Rub *et al.*, 2004). Hence, the tar removal is a key issue

---

* Published in in Applied Catalysis A: General., (2009) In press.

for downstream applications. In general, the amount of tar produced from updraft, fluidized bed and downdraft gasifiers is about 100, 10 and 1 g Nm^{-3}, respectively. A typical composition of biomass gasification tar is presented in Table 7.1 (Milne *et al.*, 1998). Of all biomass gasification tar, naphthalene is one of the most stable tar compounds and is thus difficult to decompose (Jess *et al.*, 1996; Coll *et al.*, 2001; Devi *et al.*, 2005). Hence, naphthalene was considered as a model tar compound for the investigation of biomass-derived tar reforming.

Table 7.1. Typical composition of biomass gasification (Milne *et al.*, 1998)

Compound	Percentage weight
Benzene	37.9
Toluene	14.3
Other one-ring aromatic hydrocarbons	13.9
Naphthalene	9.6
Other two-ring aromatic hydrocarbons	7.8
Three-ring aromatic hydrocarbons	3.6
Four-ring aromatic hydrocarbons	0.8
Phenolic compounds	4.6
Heterocyclic compounds	6.5
Others	1.0

Catalytic hot gas conditioning processes have been widely investigated as an attractive means for the tar elimination. These possess the potential to reduce the tar content in product gas as well as to improve the product gas composition. A number of catalysts containing noble and transition metals (e.g., Cr, Co and Ni) were employed for tar elimination (Tomishige *et al.*, 2004; Milne *et al.*, 1998). With the low cost, sufficiently high tar destruction activity along with the added advantages on the reforming of light hydrocarbons, Ni–based catalysts were intensively employed for such applications (Devi *et al.*, 2003; Magrini-Bair *et al.*, 2007). However, the major problem occurring with a Ni-based catalyst is its fast deactivation due to carbon deposition and/or metal sintering (Garcia *et al.*, 2000; Baker *et al.*, 1987). To

overcome the problem, researchers have reported different supports such as dolomite, olivine, MgO and MgO-CaO (Sato *et al.*, 2007; Swierczynski *et al.*, 2007; Miyazawa *et al.*, 2006; Srinakruang *et al.*, 2006). Yet, CeO_x-ZrO_x mixed oxides exhibited a superior resistance to carbon formation due to the high oxygen vacancy and oxygen mobility (Chen *et al.*, 2008; Pengpanich *et al.*, 2004).

Recently, it has been reported that the introduction of triple-charged ions, Mn in particular, can improve the oxygen vacancy number and the mobility of ceria-based mixed oxides (Jia *et al.*, 2008; Wu *et al.*, 2007). Such improvements would result in the reduction of coke formed on such mixed oxides. This leads us to investigate the effect of doping manganese on the steam reforming catalytic activity of naphthalene as a tar compound model over nickel supported on $Ce_{0.75}Zr_{0.25-x}Mn_xO_2$ (x = 0, 0.10, 0.20 and 0.25) mixed oxide catalysts.

7.3 Experimental

7.3.1 Catalyst Preparation

A series of mixed oxide supports $Ce_{0.75}Zr_{0.25-x}Mn_xO_2$ (x = 0, 0.10, 0.20 and 0.25) were prepared via urea hydrolysis. $Ce(NO_3)_3 \cdot 6H_2O$, $ZrOCl_2 \cdot 8H_2O$ and $Mn(NO_3)_2 \cdot 4H_2O$ were used as sources of Ce, Zr and Mn, respectively. The starting solution was prepared by mixing 0.1 M of metal salt solutions with 0.4 M of urea solution at a 2 to 1 volumetric ratio. The ratio between the metal salts was altered depending on the desired concentration: $Ce_{0.75}Zr_{0.25-x}Mn_xO_2$ in which x = 0, 0.10, 0.20 and 0.25. The synthesis procedures of catalysts have been reported elsewhere (Pengpanich *et al.*, 2002). Supported Ni catalysts (Ni = 15 wt%) were prepared by the incipient wetness impregnation method with $Ni(NO_3)_2$ solution. The as-prepared samples were dried and calcined at 500 °C for 4 h.

7.3.2 Catalyst Characterization

An X-ray diffractometer (Rigaku) equipped with a RINT 2000 wide-angle goniometer using Cu Kα radiation and a power of 40 kV × 40 mA was used for examination of the crystalline structure. The intensity data were collected at 25

°C over a 2θ range of 20–90° with a scan speed of 5° (2θ) min^{-1} and a scan step of 0.02° (2θ).

Hydrogen temperature-programmed reduction (H_2-TPR) experiments were carried out with a Micromeritics TPD/TPR 2900 apparatus equipped with a TCD detector. Prior to the reduction experiments, the sample, about 30 mg, was thermally treated under a helium stream at 100 °C to remove moisture. TPR profiles were attained by heating the samples under a 10% H_2/Ar flow (50 ml min^{-1}) from 30 °C to 900 °C at a linearly programmed rate of 10 °C min^{-1}.

The specific surface areas of the catalysts were determined by the Brunauer–Emmett–Teller (BET) method using a Quantachrome Corp. Autosorb. Prior to the analysis, the sample was outgassed to eliminate volatile adsorbents on the surface at 250 °C for 24 h.

The dispersion degree of nickel was measured by H_2-pulse chemisorption at 50 °C using an Ar flow of 50 ml min^{-1} and individual pulse of 0.1 ml (10% H_2 in Ar). For measurements, about 100 mg of sample was placed in a quartz reactor. Prior to the pulse chemisorption, the sample was reduced at 500 °C under H_2 atmosphere for 1 h. Then the sample was purged with Ar at 500 °C for 30 min and cooled to 50 °C in flowing Ar. The H_2 pulses were continued with an injection interval of 6-8 min until the areas of successive hydrogen peaks were identical. The nickel dispersion was calculated assuming the adsorption stoichiometry of one hydrogen atom per nickel surface atom.

The amount of carbon deposited on the spent catalysts was quantitatively determined by temperature-programmed oxidation (TPO) technique, which was carried out in a homemade TPO micro-reactor analyzer coupled with an FID detector. Typically, a 30 mg sample was heated from room temperature in flowing 2% O_2/He at a heating rate of 10 °C min^{-1} to 900 °C.

The morphology of carbon deposition on the spent catalysts was observed by transmission electron microscopy (TEM) using a JEOL (JEM-2010) transmission electron microscope operated at 200 kV. The sample was dispersed in absolute ethanol ultrasonically, and the solutions were then dropped on copper grids coated with a lacey carbon film.

7.3.3 Catalyst Activity Tests

Catalytic activity tests for the steam reforming of naphthalene were conducted using the atmospheric flow experimental system shown in Figure 7.1. A fixed-bed quartz tube microreactor (i.d. ∅ 6 mm) was used. Typically, ca. 100 mg of catalyst sample was packed between the layers of quartz wool. The reactor was placed in an electric furnace equipped with K-type thermocouples. The catalyst bed temperature was monitored and controlled by Shinko temperature controllers. Before the activity test, the catalyst was reduced at 500 °C for 2 h in flowing 50% H_2/He. After the reduction, the feed gas ($C_{10}H_8/H_2O$/He = 0.15 mol%/3 mol%/balance) was allowed to pass through the catalyst bed at a rate of 100 ml min^{-1} (GHSV = 20,000 h^{-1}). Measurements were carried out at a furnace temperature of 700°C. The product gases were chromatographically analyzed using a Shimadzu GC 8A equipped with a CTR I (Altech) column and a TCD detector and a Shimadzu GC 17A equipped with a HP-1 (Agilent technologies) column and an FID detector. The naphthalene conversion ($X_{C_{10}H_8}$), selectivities of carbon containing products (S_i) and the hydrogen yield (Y_{H_2}) in this work were calculated as follows:

$$X_{C_{10}H_8}(\%) = \frac{[CO]_{out} + [CO_2]_{out} + [CH_4]_{out}}{10[C_{10}H_8]} \times 100 \tag{7.1}$$

$$S_{CO}(\%) = \frac{[CO]_{out}}{[CO]_{out} + [CO_2]_{out} + [CH_4]_{out}} \times 100 \tag{7.2}$$

$$S_{CO_2}(\%) = \frac{[CO_2]_{out}}{[CO]_{out} + [CO_2]_{out} + [CH_4]_{out}} \times 100 \tag{7.3}$$

$$S_{CH_4}(\%) = \frac{[CH_4]_{out}}{[CO]_{out} + [CO_2]_{out} + [CH_4]_{out}} \times 100 \tag{7.4}$$

$$Y_{H_2}(\%) = \frac{[H_2]_{out}}{24[C_{10}H_8]} \times 100 \tag{7.5}$$

where $[C_{10}H_8]$ is the concentration of naphthalene entering the reactor, and $[CO]_{out}$, $[CO_2]_{out}$, $[CH_4]_{out}$, and $[H_2]_{out}$ are the concentrations of carbon monoxide, carbon

dioxide, methane, and hydrogen leaving the reactor, respectively. N_2 was particularly used as an internal standard for chromatographic analyses.

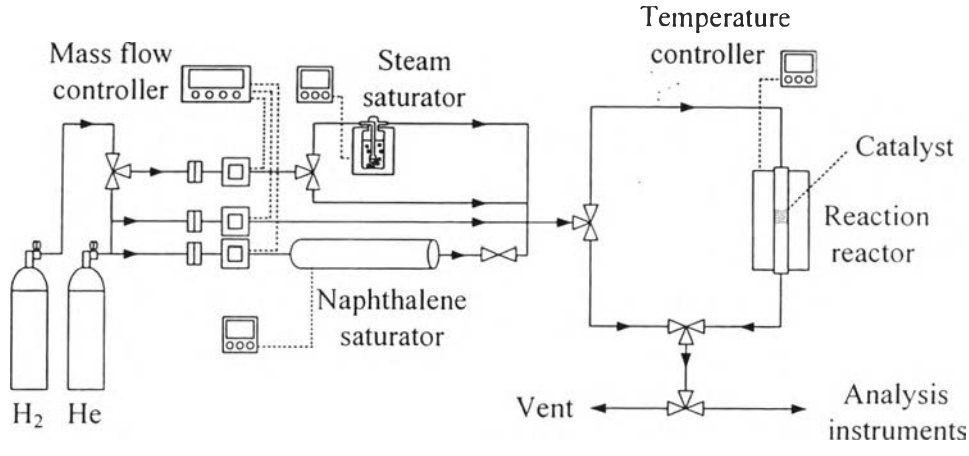

Figure 7.1 Schematic diagram of the experimental setup for naphthalene steam reforming.

7.4 Results and Discussion

7.4.1 Catalyst Characterization

7.4.1.1 XRD Analysis

The X-ray diffraction (XRD) patterns of different $Ce_{0.75}Zr_{0.25-x}Mn_xO_2$ mixed oxide catalysts impregnated with 15% Ni ($Ni/Ce_{0.75}Zr_{0.25-x}Mn_xO_2$) are presented in Figure 7.2. It was found that $Ni/Ce_{0.75}Zr_{0.25-x}Mn_xO_2$ catalysts exhibit major peaks at about 29°, 33°, 47°, and 58° (2θ) indicating the cubic fluorite structure of CeO_2. Several small peaks characteristic of NiO are observed at about 37°, 43°and 62° (2θ). No peak of either zirconia or manganese oxides is observed indicating that all zirconium cations and manganese cations dissolve in the ceria lattice. The results are similar to those reported elsewhere (Jia *et al.*, 2008; Machida *et al.*, 2000; Qi *et al.*, 2004). This might be because the ionic radii of Zr^{4+} (8.4 nm), Mn^{4+} (5.6 nm) and Mn^{3+} (6.2 nm) are smaller than that of Ce^{4+} (9.7 nm), therefore, dissolution in the ceria lattice would be possible at low doping

concentrations for both Zr and Mn. In addition, the diffraction peaks for $Ni/Ce_{0.75}Zr_{0.25-x}Mn_xO_2$ catalysts corresponding to a (111) crystallographic plane were enlarged and compared with that for pure CeO_2 as shown in the inset of Fig. 7.2. It was observed that the peaks for $Ni/Ce_{0.75}Zr_{0.25-x}Mn_xO_2$ catalysts relatively shift to a higher value as compared with that for pure CeO_2, suggesting the Zr and Mn cations are incorporated into ceria lattice. Nonetheless, it was reported that the presence of Mn_2O_3 or Mn_3O_4 was observed at high doping of Mn (Mn/(Mn+Ce) ratio > 0.75) (Machida *et al.*, 2000; Wu *et al.*, 2006; Qi *et al.*, 2004; Blanco *et al.*, 2004). Since the Mn/(Mn+Ce) ratios determined in this study were less than 0.75, we postulate that manganese cations would dissolve in the ceria lattice for the prepared $Ni/Ce_{0.75}Zr_{0.25-x}Mn_xO_2$ catalysts.

7.4.1.2 BET Surface Area and Metal Dispersion

Table 7.2 summarizes the BET surface areas, pore volumes and average pore diameters of $Ni/Ce_{0.75}Zr_{0.25-x}Mn_xO_2$ and $Ni/\alpha\text{-}Al_2O_3$ catalysts. It can be seen that the BET surface areas of $Ni/Ce_{0.75}Zr_{0.25-x}Mn_xO_2$ catalysts are in the range of 62–72 $m^2\ g^{-1}$ with average pore diameters of 6.3–7.9 nm. It should be noted that the BET surface areas of catalysts slightly decrease with increasing Mn content, except for $Ni/Ce_{0.75}Mn_{0.25}O_2$ catalyst. This result is in good agreement with that observed by Blanco *et al.* (Blanco *et al.*, 2004) indicating the relevance to the formation of the large particles of MnO_x.

The Ni dispersion degrees for $Ni/Ce_{0.75}Zr_{0.25-x}Mn_xO_2$ catalysts are higher than that for $Ni/\alpha\text{-}Al_2O_3$ catalyst (Table 7.3) suggesting that Ni particles are more highly dispersed on the $Ce_{0.75}Zr_{0.25-x}Mn_xO_2$ supports. However, such Ni dispersion degrees decrease with increasing Mn content. This result appears to be related with crystallite sizes obtained from XRD results, in which the Ni crystallite size was increased with increasing Mn loading.

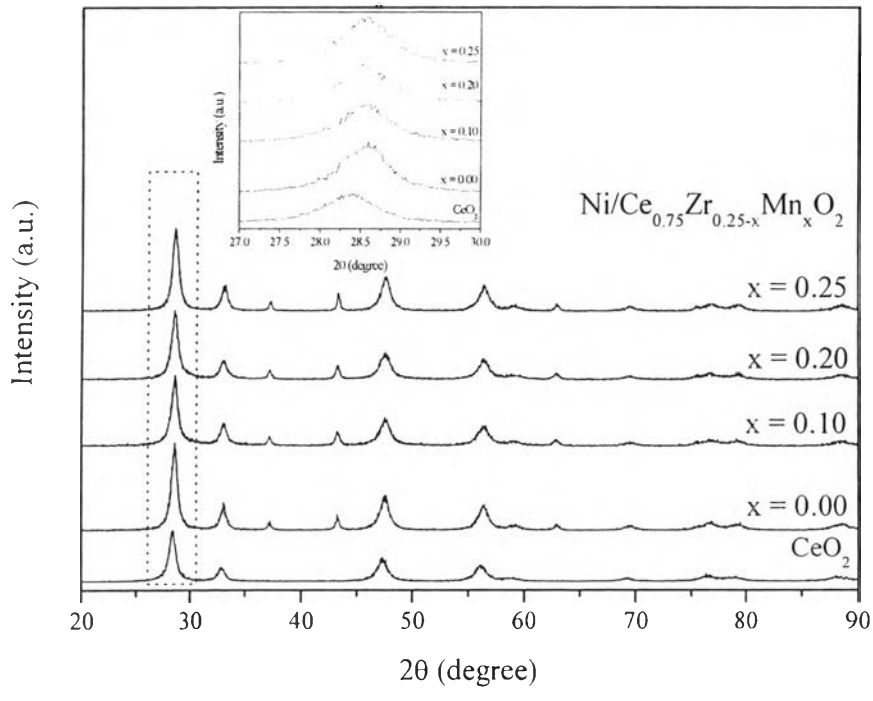

Figure 7.2 X-ray diffraction patterns for 15% $Ni/Ce_{0.75}Zr_{0.25-x}Mn_xO_2$ mixed oxide catalysts with the aging time of 50 h, and calcined at 500 °C. The enlarged (111) crystal planes of both CeO_2 and the others are presented in the inset.

Table 7.2 Textural properties of Ni-supported catalysts as measured by N_2 adsorption-desorption isotherms at –196 °C

Catalyst	BET surface area ($m^2\ g^{-1}$)	Total pore volume ($cm^3\ g^{-1}$)	Average pore diameter (nm)
15% Ni/α-Al_2O_3	5.5	0.03	18.2
15% Ni/$Ce_{0.75}Zr_{0.25}O_2$	72	0.11	7.0
15% Ni/$Ce_{0.75}Zr_{0.15}Mn_{0.10}O_2$	67	0.12	6.3
15% Ni/$Ce_{0.75}Zr_{0.05}Mn_{0.20}O_2$	62	0.13	7.9
15% Ni/$Ce_{0.75}Mn_{0.25}O_2$	72	0.12	6.4

Table 7.3 Degrees of Ni dispersion and Ni crystallite sizes of the Ni-supported catalysts

Catalyst	H_2 consumption ($\mu mol\ g_{cat}^{-1}$)	Ni dispersion (%)	Ni crystallite size (nm)
15% Ni/α-Al_2O_3	6.1	0.47	39
15% Ni/$Ce_{0.75}Zr_{0.25}O_2$	36.7	2.88	22
15% Ni/$Ce_{0.75}Zr_{0.15}Mn_{0.10}O_2$	18.6	1.46	26
15% Ni/$Ce_{0.75}Zr_{0.05}Mn_{0.20}O_2$	15.2	1.19	30
15% Ni/$Ce_{0.75}Mn_{0.25}O_2$	12.5	0.98	33

5.4.1.3 H_2-TPR

Figure 7.3 shows the H_2-TPR profiles of the $Ce_{0.75}Zr_{0.25-x}Mn_xO_2$ mixed oxides. The $Ce_{0.75}Zr_{0.25}O_2$ sample (x = 0) exhibits two distinct H_2 consumption peaks that show maxima at ca. 570 and 960 °C. The former was the reduction of surface oxygen, whereas the latter was the reduction of bulk oxygen (Pengpanich *et al.*, 2004). However, two similar peaks were observed for the $Ce_{0.75}Zr_{0.15}Mn_{0.10}O_2$ sample at ca. 510 and 940 °C, respectively. The decrease in reduction temperature resulting from the Mn incorporation suggests that manganese cations dissolve in the ceria lattice. Yet, as Mn loading was further increased, one could observe the shoulder reduction peak at ca. 270-350 °C attributed to the readily reducible small cluster surface manganese species, i.e., the reduction of MnO_2 to Mn_2O_3. The peaks appearing in the two temperature ranges of 350-420 °C and 420-510 °C were ascribed to the reduction of MnO_2/Mn_2O_3 to Mn_3O_4, and of Mn_3O_4 to MnO, respectively (Wu *et al.*, 2007; Tang *et al.*, 2006). However, it should be noted that, in this work, MnO_x was not detected by means of XRD, as discussed above.

Interestingly, the reduction temperature of surface oxygen of cerium oxide was shifted to a lower temperature of ca. 60 °C when Mn was incorporated into the mixed oxides. This suggests that the reducibility of cerium oxide is promoted probably due to the formation of solid solution between the manganese and cerium oxides resulting in the enhancement of oxygen mobility.

Figure 7.4 depicts the H_2-TPR profiles for $Ni/Ce_{0.75}Zr_{0.25-x}Mn_xO_2$ and $Ni/\alpha\text{-}Al_2O_3$ catalysts. Two H_2 consumption peaks are clearly observed for $Ni/Ce_{0.75}Zr_{0.25-x}Mn_xO_2$ catalysts as compared with that for $Ni/\alpha\text{-}Al_2O_3$ catalyst. The low temperature peak in the range of 230−350 °C can be associated with the reduction of free NiO particles and the other peak in the range of 350−550 °C can be ascribed to the reduction of complex NiO species in intimate contact with the oxide support (Pengpanich *et al.*, 2004; Roh *et al.*, 2002). This might be due to the fact that interaction between Ni and $Ce_{0.75}Zr_{0.25-x}Mn_xO_2$ supports makes the catalysts more reducible, which probably helps produce mobile oxygen during the reforming reaction. In addition, it should be noticed that the second peak reduction temperature of $Ni/Ce_{0.75}Mn_{0.25}O_2$ catalyst is shifted to lower values than those of $Ni/Ce_{0.75}Zr_{0.25-}$

$_xMn_xO_2$ catalysts, indicating its more reducibility. For the Ni/α-Al_2O_3 catalyst, only a broad peak attributed to agglomerated Ni is observed at 510 °C.

7.4.2 Catalytic Activities for Naphthalene Steam Reforming

Table 7.4 summarizes the catalytic activity of $Ce_{0.75}Zr_{0.25-x}Mn_xO_2$ supports for naphthalene steam reforming. The naphthalene conversion was slightly increased from 15.4 to 19.2% with increasing Mn content. Moreover, CO_2 selectivity and H_2 yield were also increased in a similar manner. This might be because the incorporation of Mn promotes the water-gas shift (WGS) reaction (Panagiotopoulou *et al.*, 2007; Du *et al.*, 2008). Therefore, it can be pointed out that the $Ce_{0.75}Zr_{0.25-x}Mn_xO_2$ supports themselves provide the catalytic activity for the steam reforming of naphthalene.

Table 7.5 presents the selectivities of carbon containing products, hydrogen yield, and H_2/CO molar ratio for naphthalene steam reforming over Ni/$Ce_{0.75}Zr_{0.25-x}Mn_xO_2$ catalysts. It was found that the steam reforming products are mainly CO, CO_2 and H_2 for the Ni/$Ce_{0.75}Zr_{0.25-x}Mn_xO_2$ (x = 0.10, 0.20 and 0.25) with H_2/CO ratios of 2.3-2.6 while those over the Ni/$Ce_{0.75}Zr_{0.25}O_2$ are CO, CO_2, H_2, and a trace of CH_4 with a H_2/CO ratio of 1.8. Since the increases in both CO_2 selectivity and H_2/CO ratio are observed for the Mn-containing catalysts, such phenomena conform to the existence of the WGS reaction over the Ni/$Ce_{0.75}Zr_{0.25-x}Mn_xO_2$ (x = 0.10, 0.20 and 0.25) mixed oxide catalysts.

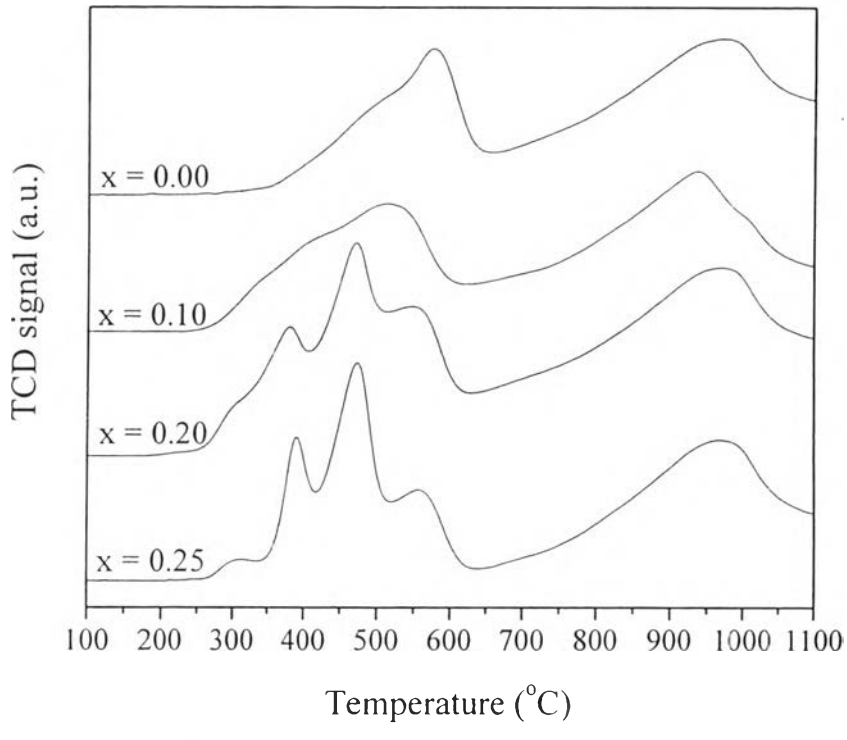

Figure 7.3 H_2-TPR profiles of the $Ce_{0.75}Zr_{0.25-x}Mn_xO_2$ mixed oxide samples.

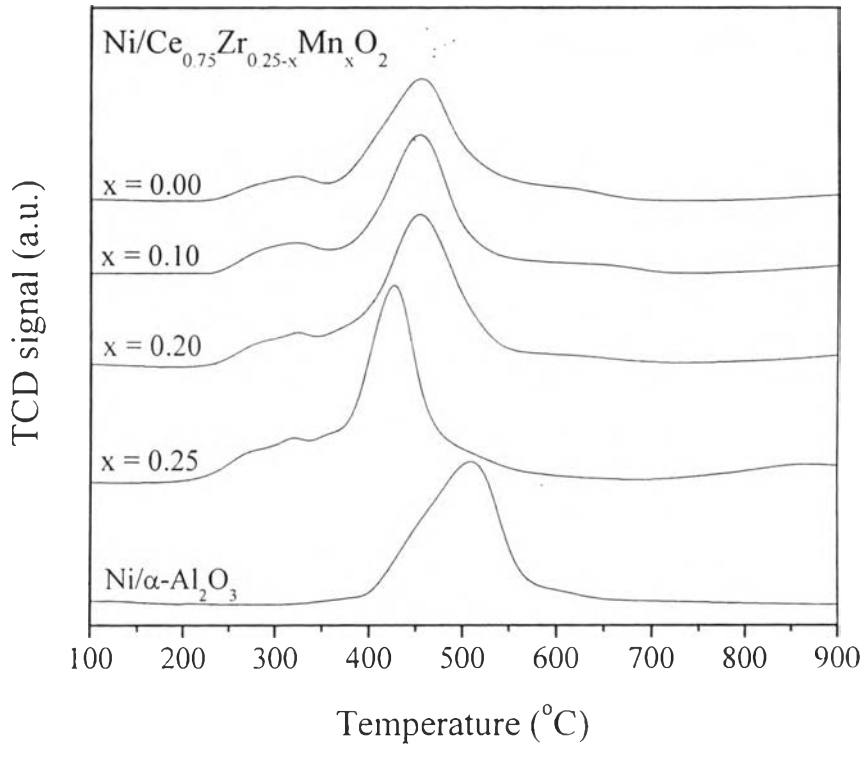

Figure 7.4 H_2-TPR profiles of the 15% $Ni/Ce_{0.75}Zr_{0.25-x}Mn_xO_2$ mixed oxide and 15% Ni/α-Al_2O_3 catalysts.

Table 7.4 Naphthalene steam reforming activity of $Ce_{0.75}Zr_{0.25-x}Mn_xO_2$ supports (reaction temperature = 700 °C; time on stream = 6 h; S/C ratio = 2.0)

Catalyst	X (%)	S_{CO} (%)	S_{CO_2} (%)	S_{CH_4} (%)	Y_{H_2} (%)
$Ce_{0.75}Zr_{0.25}O_2$	15.4	72.7	27.2	0.1	7.2
$Ce_{0.75}Zr_{0.15}Mn_{0.10}O_2$	16.0	67.2	32.7	0.1	10.6
$Ce_{0.75}Zr_{0.10}Mn_{0.15}O_2$	17.4	61.3	38.5	0.2	12.4
$Ce_{0.75}Mn_{0.25}O_2$	19.2	37.4	62.3	0.3	23.3

Table 7.5 Naphthalene steam reforming activity of $Ni/Ce_{0.75}Zr_{0.25-x}Mn_xO_2$ catalysts (reaction temperature = 700 °C; time on stream = 6 h; S/C ratio = 2.0; naphthalene conversion = 1)

Catalyst	S_{CO} (%)	S_{CO_2} (%)	S_{CH_4} (%)	Y_{H_2} (%)	H_2/CO ratio
15% $Ni/Ce_{0.75}Zr_{0.25}O_2$	97.6	2.2	0.2	72.9	1.8
15% $Ni/Ce_{0.75}Zr_{0.15}Mn_{0.10}O_2$	80.0	20.0	0	75.4	2.3
15% $Ni/Ce_{0.75}Zr_{0.10}Mn_{0.15}O_2$	74.3	25.7	0	76.3	2.4
15% $Ni/Ce_{0.75}Mn_{0.25}O_2$	75.5	24.5	0	76.3	2.6

7.4.3 Effect of the Steam-to-Carbon Ratio

The influence of the steam-to-carbon (S/C) ratio on the catalytic activity of $Ni/Ce_{0.75}Zr_{0.25}O_2$ and $Ni/Ce_{0.75}Zr_{0.15}Mn_{0.10}O_2$ catalysts was investigated by varying the S/C ratios from 2.0 to 5.0 at 700 °C. The naphthalene was completely converted when employing both catalysts regardless of the S/C ratio. As observed in Figure 7.5, the H_2 yield for the $Ni/Ce_{0.75}Zr_{0.15}Mn_{0.10}O_2$ is slightly higher than that for the $Ni/Ce_{0.75}Zr_{0.25}O_2$ at a given S/C ratio due to the influence of doping Mn into the ceria lattice on the WGS reaction. The high amounts of H_2 and CO_2 were produced at high S/C ratios via the WGS reaction since a high steam partial pressure pushes the WGS equilibrium towards the H_2 and CO_2 formation. It is evident that the H_2 yield attained experimentally from the $Ni/Ce_{0.75}Zr_{0.15}Mn_{0.10}O_2$ catalyst seems to reach the equilibrium value because of the pronounced effect of WGS reactions.

7.4.4 Carbon Formation

The catalytic activities and stabilities of $Ni/Ce_{0.75}Zr_{0.25-x}Mn_xO_2$ catalysts for steam reforming of naphthalene were compared with those of Ni/α-Al_2O_3 catalyst. It was found that the complete naphthalene conversions of $Ni/Ce_{0.75}Zr_{0.25-x}Mn_xO_2$ (x = 0, 0.10, 0.20, 0.25) catalysts remained unchanged for at least 6 h on stream whereas a rapid deactivation was observed for Ni/α-Al_2O_3 catalyst after 2 h on stream as shown in Figure 7.6. This suggests that the $Ni/Ce_{0.75}Zr_{0.25-x}Mn_xO_2$ catalysts are rather highly active and are stable for the steam reforming of naphthalene. The synergetic effect of an ease of reducibility and a good oxidation ability of the $Ce_{0.75}Zr_{0.25-x}Mn_xO_2$ supports appears to play a role in promoting the oxidation of carbon precursors on the nickel surface.

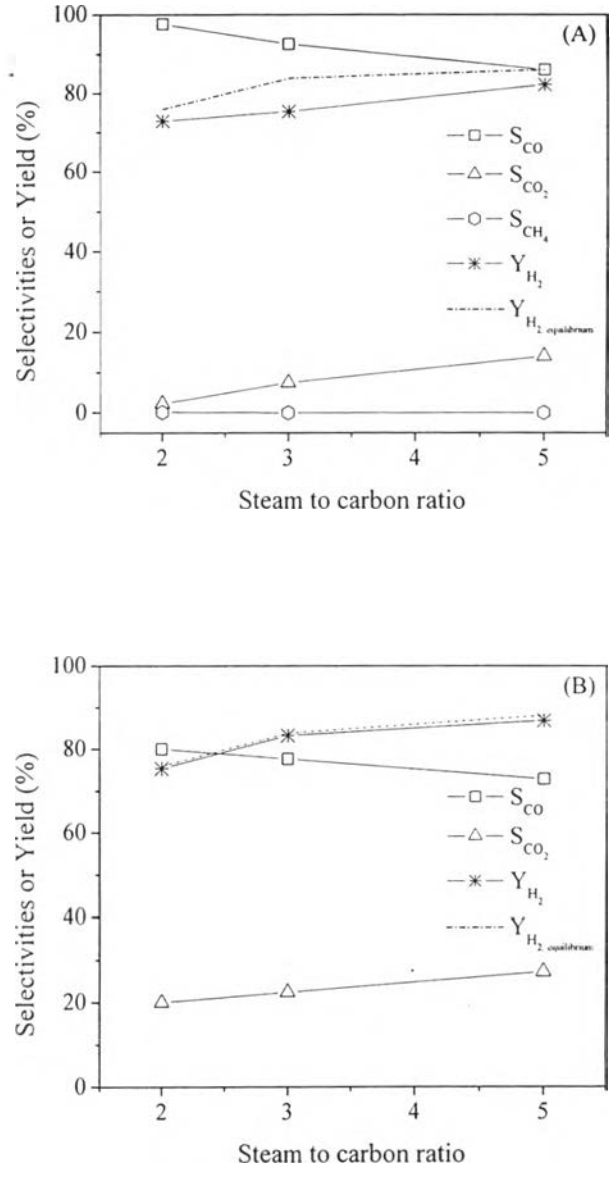

Figure 7.5 Effect of S/C ratio on the selectivities of carbon containing products and hydrogen yield over: (A) 15% $Ni/Ce_{0.75}Zr_{0.25}O_2$, (B) 15% $Ni/Ce_{0.75}Zr_{0.15}Mn_{0.10}O_2$.

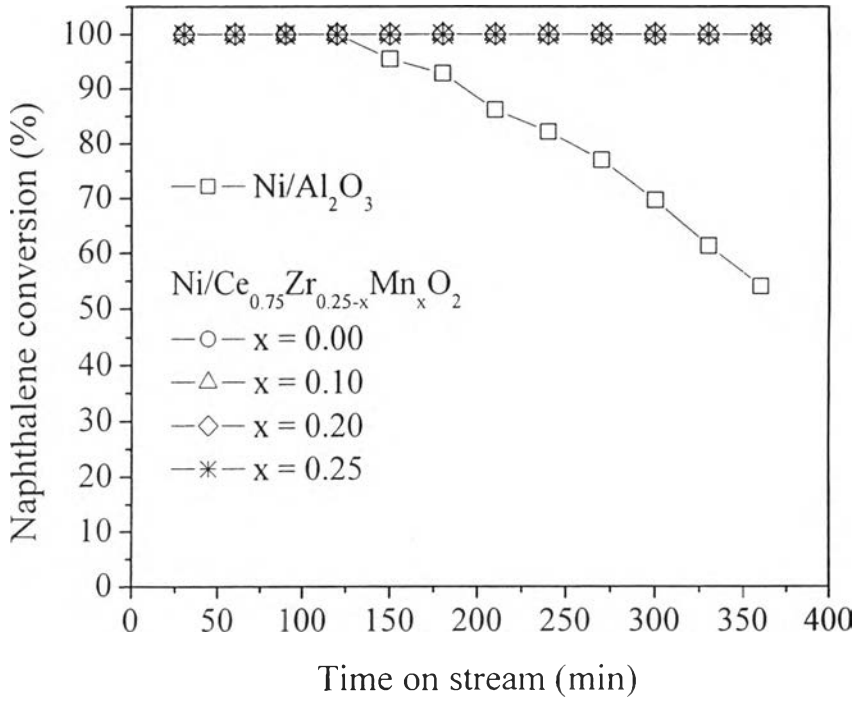

Figure 7.6 Catalytic activity for naphthalene steam reforming over 15% $Ni/Ce_{0.75}Zr_{0.25-x}Mn_xO_2$ mixed oxide and 15% $Ni/\alpha\text{-}Al_2O_3$ catalysts; with a gas mixture composed of 1,500 ppmv $C_{10}H_8$, S/C ratio = 2.0 and T = 700 °C.

Figure 7.7 shows the TPO profiles for the spent $Ni/Ce_{0.75}Zr_{0.25-x}Mn_xO_2$ and $Ni/\alpha\text{-}Al_2O_3$ catalysts after being exposed to the naphthalene steam reforming at 700 °C for 6 h on stream. The two types of carbon formation on the spent $Ni/Ce_{0.75}Zr_{0.25}O_2$ and $Ni/\alpha\text{-}Al_2O_3$ catalysts are identical in nature according to the profiles at low and high temperatures. The small peak at a lower temperature of ca. 325 °C was attributed to the carbidic carbon and the other peak at a higher temperature of ca. 680 °C corresponded to the filamentous carbon (Swierczynski *et al.*, 2007; Vargas *et al.*, 2005). However, it is worth noting that the high temperature peaks seem to disappear from those of the spent Mn containing catalysts. The amounts of carbon deposited on the spent catalysts determined as summarized in Table 7.6 indicate that the Mn-doped catalysts, $Ni/Ce_{0.75}Zr_{0.25-x}Mn_xO_2$ (x = 0.10, 0.20, 0.25), possess much lower amounts of carbon formed (ca. 1.1 ± 0.3 mg g_{cat}^{-1}) as compared to the amounts formed on the $Ni/\alpha\text{-}Al_2O_3$ and $Ni/Ce_{0.75}Zr_{0.25}O_2$ catalysts (63.4 and 26.7 mg g_{cat}^{-1}, respectively). The results conform to the TEM images illustrated in Figure 7.8. The spent $Ni/\alpha\text{-}Al_2O_3$ and $Ni/Ce_{0.75}Zr_{0.25}O_2$ catalysts are fully covered with filamentous carbon (Figure 7.8 (A) and 7.8 (B)), whereas no such carbon is observed on the $Ni/Ce_{0.75}Zr_{0.15}Mn_{0.10}O_2$ catalyst (Figure 7.8 (C)). We believe that the modification of $Ni/CeO_2\text{-}ZrO_2$ catalysts with Mn incorporation helps prevent the carbon deposition by promoting the surface carbon gasification and/or WGS reaction.

Table 7.6 Total amounts of carbon deposited on catalysts via the naphthalene steam reforming; after 6 h on stream, at 700 °C and S/C ratio of 2.0

Catalyst	Carbon formation (mg g_{cat}^{-1})
15% $Ni/\alpha\text{-}Al_2O_3$	63.4
15% $Ni/Ce_{0.75}Zr_{0.25}O_2$	26.7
15% $Ni/Ce_{0.75}Zr_{0.15}Mn_{0.10}O_2$	0.8
15% $Ni/Ce_{0.75}Zr_{0.05}Mn_{0.20}O_2$	1.2
15% $Ni/Ce_{0.75}Mn_{0.25}O_2$	1.4

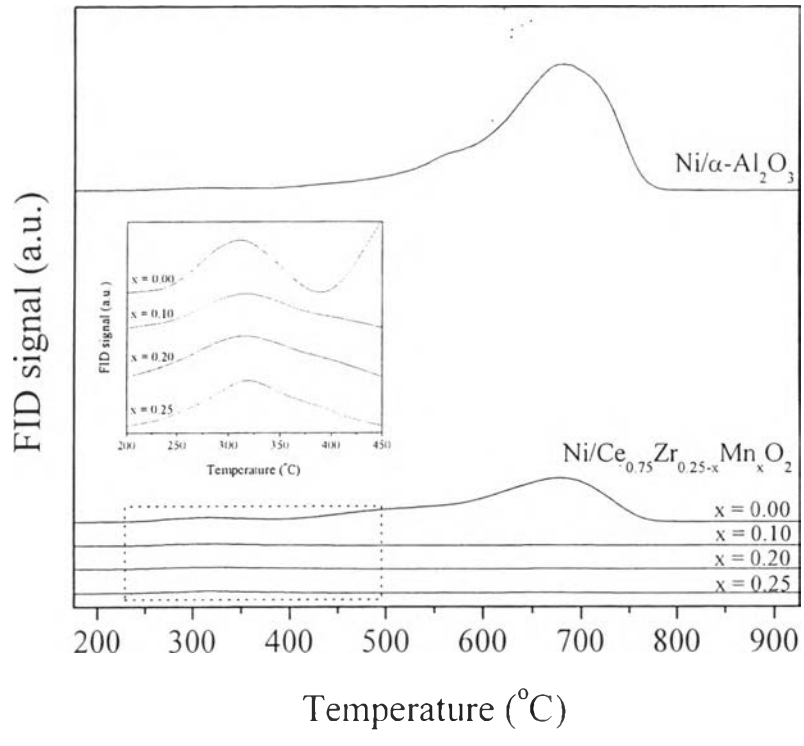

Figure 7.7 TPO profiles of the spent catalysts (15% $Ni/Ce_{0.75}Zr_{0.25-x}Mn_xO_2$ mixed oxide and 15% $Ni/\alpha-Al_2O_3$) after exposure to reaction at 700 °C for 6 h.

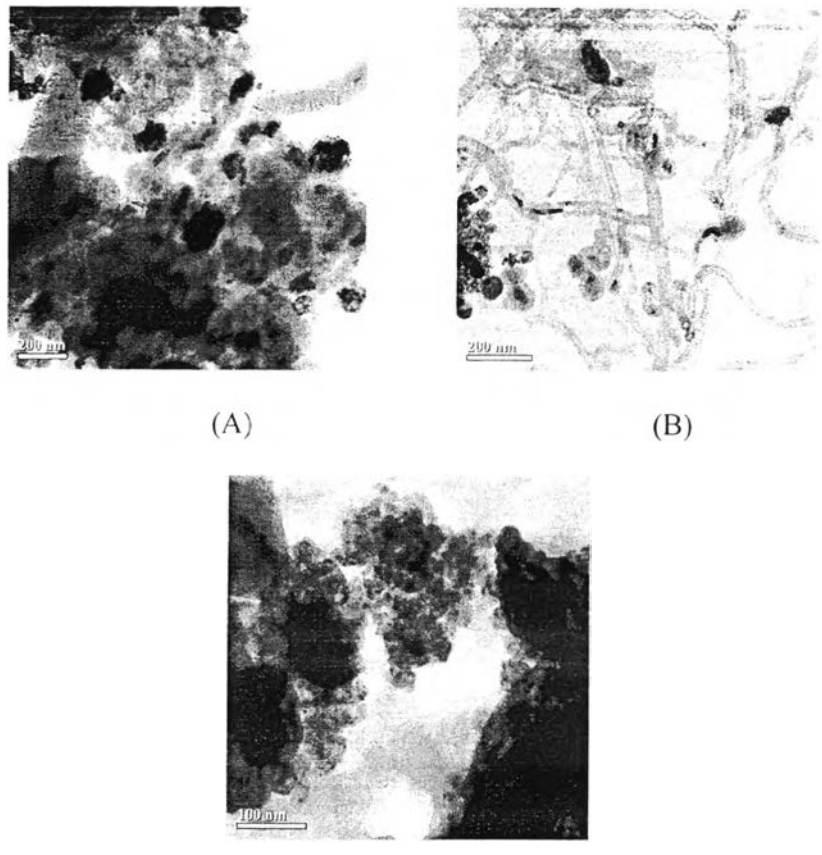

(A) (B)

(C)

Figure 7.8 TEM images of the spent catalysts: (A) 15% Ni/α-Al_2O_3, (B) 15% Ni/$Ce_{0.75}Zr_{0.25}O_2$, (C) 15% Ni/$Ce_{0.75}Zr_{0.15}Mn_{0.10}O_2$.

7.5 Conclusions

The $Ni/Ce_{0.75}Zr_{0.25-x}Mn_xO_2$ (x= 0, 0.10, 0.20, and 0.25) mixed oxide catalysts exhibit high activities and stabilities for naphthalene steam reforming. The incorporation of Mn into $Ce_{0.75}Zr_{0.25}O_2$ mixed oxide is able to modify the redox properties of the mixed oxide support, resulting in the improvement of catalytic properties of the $Ni/Ce_{0.75}Zr_{0.25}O_2$ catalyst. Furthermore, the presence of Mn in the catalysts studied results in the dramatic decrease in carbon deposition due to the reduction of filamentous carbon by retarding the solubility of carbon in Ni particles as well as by promoting the oxidation of intermediates or precursor of deposited carbon.

7.6 Acknowledgements

This work was supported by the Thailand Research Fund (under Waste-to-Energy project and Royal Golden Jubilee Ph.D. Program: Grant 0170/46), by the Research Unit for Petrochemical and Environmental Catalysis, Ratchadapisek Somphot Endowment Fund, and by the National Center of Excellence for Petroleum, Petrochemicals and Advanced Materials, Chulalongkorn University.

7.7 References

Abu El-Rub, Z., 2004. Review of catalysts for tar elimination in biomass gasification processes. Industrial Engineering Chemistry Production Research Development, 43, 6911-6919.

Baker, E.G., Mudge, L.K., Brown, M.D. (1987) Steam gasification of biomass with nickel secondary catalysts. Industrial and Engineering Chemistry Research, 26, 1335-1339.

Blanco, G., Cauqui, M.A., Delgado, J.J., Galtayries, A., Pérez-Omil, J.A., Rodríguez-Izquierdo, J.M. (2004) Preparation and characterization of Ce–Mn–O composites with applications in catalytic wet oxidation processes. Surface and Interface Analysis, 36, 752-755.

Chen, J., Wu, Q., Zhang, J., Zhang, J. (2008) Effect of preparation methods on structure and performance of $Ni/Ce_{0.75}Zr_{0.25}O_2$ catalysts for CH_4–CO_2 reforming. Fuel, 87, 2901-2907.

Coll, R., Salvadó, J., Farriol, X., Montané D. (2001) Steam reforming model compounds of biomass gasification tars: conversion at different operating conditions and tendency towards coke formation. Fuel Processing Technology, 74, 19-31.

Devi, L., Ptasinski, K.J., Janssen, F.J.J.G. (2003) A review of the primary measures for tar elimination in biomass gasification processes. Biomass and Bioenergy, 24, 125-140.

Devi, L., Ptasinski, K.J., Janssen, F.J.J.G., van Paasen, S.V.B., Bergman, P.C.A., Kiel, J.H.A. (2005) Catalytic decomposition of biomass tars: use of dolomite and untreated olivine. Renewable Energy, 30, 565-587.

Du, X., Yuan, Z., Cao, L., Zhang, C., Wang, S. (2008) Water gas shift reaction over Cu–Mn mixed oxides catalysts: Effects of the third metal. Fuel Processing Technology, 89, 131-138.

Garcia, L., French, R., Czernik, S., Chornet, E. (2000) Catalytic steam reforming of bio-oils for the production of hydrogen: effect of catalyst composition. Applied Catalysis A: General, 201, 225-239.

Jess, A. (1996) Catalytic upgrading of tarry fuel gases: A kinetic study with model components. Chemical Engineering and Processing, 35, 487-494.

Jia, L., Shen, M., Hao, J., Rao, T., Wang, J. (2008) Dynamic oxygen storage and release over $Mn_{0.1}Ce_{0.9}O_x$ and $Mn_{0.1}Ce_{0.6}Zr_{0.3}O_x$ complex compounds and structural characterization. Journal of Alloys and Compounds, 454, 321-326.

Machida, M., Uto, M., Kurogi, D., Kijima, T. (2000) MnO_x-CeO_2 binary oxides for catalytic NO_x sorption at low temperatures. sorptive removal of NO_x. Chemistry of Materials, 12, 3158-3164.

Magrini-Bair, K.A., Czernik, S., French, R., Parent, Y.O., Chornet, E., Dayton, D.C., Feik, C., Bain, R. (2007) Fluidizable reforming catalyst development for conditioning biomass-derived syngas. Applied Catalysis A: General, 318, 199-206.

Milne, T.A., Abatzoglou, N., Evans, R.J. (1998) Biomass gasifier 'tars': Their nature, formation and conversion. NREL/TP-570-25357, National Renewal Energy Laboratory.

Miyazawa, T., Kimura, T., Nishikawa, J., Kado, S., Kunimori, K., Tomishige, K. (2006) Catalytic peerformance of supported Ni catalysts in partial oxidation and steam reforming of tar derived from the pyrolysis of wood biomass. Catalysis Today, 115, 254-262.

Panagiotopoulou, P., Kondarides, D.I. (2007) A comparative study of the water-gas shift activity of Pt catalysts supported on single (MO_x) and composite (MO_x/Al_2O_3, MO_x/TiO_2) metal oxide carriers. Catalysis Today, 127, 319-329.

Pengpanich, S., Meeyoo, V., Risksomboon, T., Bunyakiat, K. (2002) Catalytic oxidation of methane over CeO_2-ZrO_2 mixed oxide solid solution catalysts prepared via urea hydrolysis. Applied Catalysis A: General, 234, 221-233.

Pengpanich, S., Meeyoo, V., Risksomboon, T. (2004) Methane partial oxidation over Ni/CeO_2–ZrO_2 mixed oxide solid solution catalysts. Catalysis Today, 93-95, 95-105.

Qi, G., Yang, R.T., Chang, R. (2004) MnO_x-CeO_2 mixed oxides prepared by co precipitation for selective catalytic reduction of NO with NH_3 at low temperatures. Applied Catalysis B: Environmental, 51, 93-106.

Roh, H.-S., Jun, K.-W., Dong, W.-S., Chang, J.-S., Park, S.-E., Joe, Y.-I. (2002) Highly active and stable Ni/Ce–ZrO2 catalyst for H_2 production from methane. Journal of Molecular Catalysis A: Chemical, 181, 137-142.

Sato, K., Fujimoto, K. (2007) Development of new nickel based catalyst for tar reforming with superior resistance to sulfur poisoning and coking in biomass gasification. Catalysis Communications, 8, 1697-1701.

Srinakruang, J., Sato, K., Vitidsant, T., Fujimoto, K. (2006) Highly efficient sulfur and coking resistance catalysts for tar gasification with steam. Fuel, 85, 2419-2426.

Sutton, D., Kelleher, B., Ross, J.R.H. (2001) Review of literature on catalysts for biomass gasification. Fuel Processing Technology, 73, 155-173.

Swierczynski, D., Libs, S., Courson, C., Kiennemann, A. (2007) Steam reforming of tar from a biomass gasification process over Ni/olivine catalyst using toluene as a model compound. Applied Catalysis B: Environmental, 74, 211-222.

Tang, X., Li, Y., Huang, X., Xu, Y., Zhu, H., Wang, J., Shen, W. (2006) MnO_x-CeO_2 mixed oxide catalysts for complete oxidation of formaldehyde: Effect of preparation method and calcination temperature. Applied Catalysis B: Environmental, 62, 265-273.

Tomishige, K., Asadullah, M., Kunimori, K. (2004) Syngas production by biomass gasification using $Rh/CeO_2/SiO_2$ catalysts and fluidized bed reactor. Catalysis Today, 89, 389-403.

Vargas, J.C., Lib, S., Roger, A.-C., Kiennemann, A. (2005) Study of Ce-Zr-Co fluorite-type oxide as catalysts for hydrogen production by steam reforming of bioethanol. Catalysis Today, 107-108, 417-425.

Wu, X., Liang, Q., Weng, D. (2006) Effect of manganese doping on oxygen storage capacity of ceria- zirconia mixed oxides. Journal of Rare Earths, 24, 549-553.

Wu, X., Liang, Q., Weng, D., Fan, J., Ran, R. (2007) Synthesis of CeO_2–MnO_x mixed oxides and catalytic performance under oxygen-rich condition. Catalysis Today, 126, 430-435.

Zhang, R., Brown, R.C., Suby, A., Cummer, K. (2004) Catalytic destruction of tar in biomass derived producer gas. Energy Conversion and Management, 45, 995-1014.